HHS Public Access

Author manuscript

Nano Lett. Author manuscript; available in PMC 2024 May 31.

Published in final edited form as:

Nano Lett. 2024 May 22; 24(20): 6112–6116. doi:10.1021/acs.nanolett.4c01280.

Simultaneous Mapping of Electrocatalytic Activity and Selectivity via Hybrid Scanning Electrochemical Probe Microscopy

C. Hyun Ryu,

Department of Chemistry, The University of Texas at Austin, Austin, Texas 78712, United States

Hang Ren

Department of Chemistry, The University of Texas at Austin, Austin, Texas 78712, United States

Center for Electrochemistry and Texas Materials Institute, The University of Texas at Austin, Austin, Texas 78712, United States

Abstract

Nanoscale scanning electrochemical probe microscopy started to elucidate the heterogeneity of electrocatalytic activity at electrode surfaces. However, understanding the heterogeneity in product selectivity, another crucial aspect of interfacial reactivity, remains challenging. Herein, we introduce a method combining scanning electrochemical microscopy (SECM) and scanning electrochemical cell microscopy (SECCM) to enable the spatially resolved mapping of both activity and selectivity in electrocatalysis. A dual-channel nanopipette probe was developed: one channel for activity mapping and the other for product detection with a high collection efficiency (>95%) and sensitivity. Simultaneous mapping of activity and selectivity in the oxygen reduction reaction (ORR) is demonstrated. Combined with colocalized crystal orientation mapping, we uncover the local electrocatalytic performance of ORR at different facets on polycrystalline Pt and Au. The high-resolution selectivity mapping enabled by our method with colocalized structural characterization can provide structure–activity-selectivity relationships that are often unavailable in ensemble measurement, holding promise for understanding key structural motifs controlling interfacial reactivity.

Corresponding Author: Hang Ren – *Department of Chemistry, The University of Texas at Austin, Austin, Texas 78712, United States; Center for Electrochemistry and Texas Materials Institute, The University of Texas at Austin, Austin, Texas 78712, United States*; hren@utexas.edu.

Notes

The authors declare no competing financial interest.

Complete contact information is available at: https://pubs.acs.org/10.1021/acs.nanolett.4c01280

ASSOCIATED CONTENT

Supporting Information

The Supporting Information is available free of charge at https://pubs.acs.org/doi/10.1021/acs.nanolett.4c01280.

Experimental section, probe fabrication, finite element simulation, probe characterization, more mapping data (PDF)

Movie S1: voltammetric movie of substrate current and n-value on Au and Pt (MP4)

Movie S2: voltammetric movie of substrate current and n-value on Au and Pt (MP4)

Movie S3: voltammetric movie of substrate current and n-value on Au and Pt (MP4)

Movie S4: voltammetric movie of substrate current and n-value on Au and Pt (MP4)

Movie S5: voltammetric movie of substrate current and n-value on Au and Pt (MP4)

Graphical Abstract.

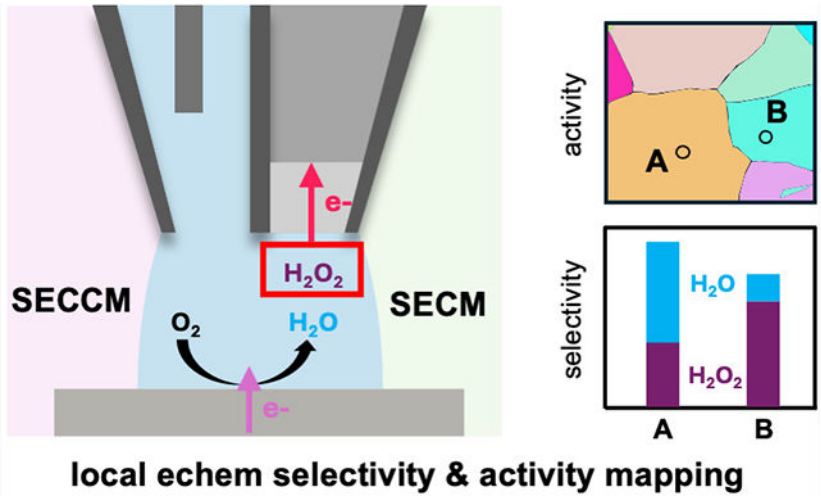

Keywords

SECCM; SECM; Electrochemical Imaging; Heterogeneity; Oxygen Reduction Reaction; Nanoelectrochemistry

Understanding the reactivity of electrochemical interfaces, particularly those involved in electrocatalytic reactions such as oxygen reduction reaction (ORR) and CO_2 reduction reaction (CO_2RR), is critical for advancing electrochemical energy storage and conversion technology.[1,2] Traditional ensemble bulk electrochemistry has been used to examine the structure–activity relationship at these interfaces.[3–5] However, the electrode surface contains heterogeneities of different length scales, while conventional measurements average the activity over the entire interface, obscuring the detailed activity at specific sites. In some cases, the activity of the entire surface can be dominated by a few local active sites, which escape the ensemble measurement. Therefore, it is challenging to determine the true structure–activity relationship using conventional electrochemical techniques.

Scanning electrochemical microscopy (SECM) is one of the first developed techniques in scanning electrochemical probe microscopy.[2,6] It uses an ultramicroelectrode or nanoelectrode as a probe to observe electrochemical behavior at micro- and nanoscales. Recently, scanning electrochemical cell microscopy (SECCM) has gained popularity due to the high nanometer resolution and ease of probe fabrication.[7–9] In SECCM, a glass nanopipet filled with electrolyte solution is used as the probe. The probe is brought to make ionic contact with the substrate electrode through the nanodroplet at the end of the probe, creating a small electrode area that is on a submicron to nanometer scale. The current from the nanodroplet cell represents a direct measurement of the local electrochemical activity. Scanning the nanopipette probe across the surface enables the mapping of electrochemical activity at the nanoscale and single entity levels.[7,10–13] When combined with colocalized structural characterization, the correlation between the local activity and local structures, including crystal orientation and defects such as grain boundaries, can be elucidated.

In addition, the heterogeneity in the activity between and within single nanoparticle electrocatalysts can also be better visualized.[10,13]

Although scanning electrochemical probe microscopy has yielded great success in mapping electrocatalytic activity, measuring local selectivity in electrocatalysis remains a challenge. This is a crucial issue to address because conventional ensemble measurements of electrocatalytic selectivity suffer from the same problem of heterogeneity at the electrode surface.[5] Adding the capability of selectivity mapping into SECCM can help provide new information about the structural motifs that control the reaction selectivity at electrochemical interfaces.

Herein, we report the development of a hybrid SECCM-SECM mapping method that combines the advantages of both SECM and SECCM, enabling the mapping of electrocatalytic activity and selectivity. A dual-channel nanopipet is modified: One channel is filled with an electrolyte solution to measure the activity at the substrate electrode as in SECCM, while the second channel is transformed into a local tip electrode for measuring reaction products as in SECM. The oxygen reduction reaction (ORR) is chosen as the model reaction to demonstrate the mapping of local activity and selectivity, and the product of H_2O_2 is electrochemically detected. Combined with colocalized crystal orientation mapping, the dependence of activity and selectivity on the local crystal orientation is determined using polycrystalline Au and Pt.

The probe was fabricated from a dual-channel nanopipet (~700 nm in diameter) by carbon pyrolysis in one channel,[14,15] followed by electrodeposition of Pt on carbon. The second channel is left empty for solution filling. The fabrication procedure is described in the SI section S2, and characterization via voltammetry and electron microscopy is shown in SI section S4. In a typical experiment, the droplet probe is in contact with the substrate electrode, as illustrated in Scheme 1. A potential is applied between the substrate and the Ag/AgCl quasi-reference/counter electrode (QRCE) placed in the solution channel. Voltammetric scanning of the substrate allows measurement of the local electrochemical activity defined by the droplet substrate interface as in SECCM. Meanwhile, the tip electrode in the hybrid probe can be held at a potential to electrochemically detect the product generated within the nanodroplet cell. As a result, the electrochemical activity and selectivity can be measured locally from the substrate electrode and the tip electrode currents, respectively. The same measurement can be repeated across the substrate surface by scanning the probe on the substrate electrode, allowing for the mapping of electrocatalytic activity and selectivity.

We first use finite element simulation to validate the collection efficiency of the hybrid probe, which measures the fraction of product generated at the substrate that is electrochemically detected at the tip electrode. In the simulation (Figure S5), a collection efficiency of 90% is obtained, suggesting that most solution products can be detected in this hybrid SECM–SECCM method. We also experimentally verify the collection efficiency using a water-soluble ferrocene derivative, (ferrocenylmethyl)trimethylammonium ($FcTMA^+$), as the redox molecule. The substrate electrode potential was swept positively by voltammetry to oxidize $FcTMA^+$ to $FcTMA^{2+}$, while the tip electrode was held at 0.00

V to reduce $FcTMA^{2+}$ back to $FcTMA^{+}$. As shown in Figure 1a, the current from both the substrate and the tip increases as the substrate electrode potential becomes more positive. Both reach limiting currents with similar absolute values (~0.2 nA), indicating that the tip electrode can collect most of the solution products generated by the substrate electrode. The ratio of the limiting current on the tip to that on the substrate yields a collection efficiency of 95.5%. The reproducibility of the collection efficiency is further demonstrated in 422 consecutive local voltammetric experiments on glassy carbon. Figure 1b shows a collection efficiency of 97.5 ± 0.6% (mean ± standard deviation), with all locations showing >95% collection efficiency, demonstrating good reproducibility. The SEM image with footprints corresponding to the mapping area is shown in Figure 1c, which shows the consistency of the droplet contact with the substrate electrode. We also experimentally demonstrate that the collection efficiency does not strongly depend on the distance between the substrate and the tip (e.g., < 2% in over ~300 nm, see Figure S6), which explains the consistency of collection efficiency during the mapping (Figure 1b).

We now demonstrate that our probe can measure both the activity and the selectivity locally using ORR on Au and Pt as the model reaction. The potential on the substrate electrode is swept negatively to induce ORR, while the Pt tip electrode is held at 0.80 V to collect H_2O_2 oxidatively. This tip potential is effective for H_2O_2 oxidation, as shown by its voltammetry in a H_2O_2 solution (Figure S7). The voltammetric results using the new hybrid probe show that a mixture of H_2O_2 and H_2O is generated from ORR on Au (Figure S9a–c), while H_2O is the primary product on Pt (Figure S9d–f), consistent with previous reports.[16–19] The selectivity of ORR is quantified by the average number of electrons (n) via:

$$n = \frac{4 \times i_{sub}}{i_{sub} + \frac{i_{tip}}{\eta}} \quad (1)$$

In eq 1, i_{sub} and i_{tip} are the substrate and tip currents, respectively, and η is the collection efficiency (i.e., ~95%). The n value varies between 2 and 4, with 2 representing 100% H_2O_2 as the product, and four representing 100% H_2O as the product. Example plots of the n value as a function of substrate potential on Au and Pt are shown in Figures S11 and S12.

We further demonstrated spatially resolved mapping of the ORR activity and selectivity on polycrystalline Au in the hybrid SECCM–SECM mapping experiment via a pseudo-single-crystal electrochemistry approach.[20] The mapping procedure is illustrated in Scheme S3. Figure 2a shows the SEM image of the region of polycrystalline Au after activity-selectivity mapping. The contrast in the SEM image indicates different grains. In addition, 289 footprints after the hopping scan can be observed in the image. Each footprint maintained an eclipse shape with ~350 and ~200 nm radii for the major and minor axes (Figure S1). The ORR activity is confirmed by the substrate current at $E_{sub} = -0.42$ V (Figure 2b), and similar current values are clustered in different regions. A similar trend is observed in the tip current for the H_2O_2 collection (Figure 2c). These clustered regions correlate well with different crystal grains, as shown in the SEM image (Figure 2a). The crystal orientation of seven grains was obtained by electron backscatter diffraction (EBSD) as shown in Figure 2e.

Grains III, V, and VII, close to (011) as shown in the inverse pole figure (IPF) in Figure 2f, exhibited significantly higher current, indicating higher ORR activity. Grain I, which is close to (111), showed the lowest ORR activity, consistent with previous studies on single-crystal electrodes.[19] Grains II, IV, and VI, which have crystallographic characteristics of (100) and (111), showed intermediate ORR activity.

A heatmap of selectivity (i.e., n value) at $E_{sub} = -0.42$ V in the positive scan is shown in Figure 2d. Grains III, V, and VII, close to (011), showed lower n values than other nearby grains, indicating that more H_2O_2 is generated at those surfaces. In contrast, grain VI, which is close to the high index plane of (411), showed the highest n value, suggesting a more complete reduction to H_2O. These results indicated that selectivity did not follow the trends of the ORR activity, emphasizing the importance of simultaneous local measurement of activity and selectivity. Voltammetric movies showing the substrate current map and selectivity map at various substrate potentials are included as Movies S1 and S2. Interestingly, we observed little difference in n across different grains during the negative going scan, which is further discussed in the SI (section S6).

Last, we map the ORR activity and selectivity of polycrystalline Pt. Figure 3a shows 289 footprints on the polycrystalline Pt sample. Current heatmaps ($E_{sub} = -0.50$ V) of local activity (i.e., i_{sub}) and H_2O_2 collection (i_{tip}) are shown in Figure 3b and c. The current heatmaps correlate with the grain image from the SEM image (Figure 3a) and EBSD (Figure 3e). The substrate current at −0.50 V varies between −130 and 260 pA, while the H_2O_2 collection current is consistently lower than 5 pA, suggesting very little H_2O_2 is generated. The quantitative selectivity of ORR is shown by the n value heatmap in Figure 3d, suggesting small but different selectivity across different Pt grains. Grains VI and VIII show relatively lower n values than other grains, although all n values were higher than 3.9, consistent with the expected ORR selectivity on Pt. In the negative going scan on the polycrystalline Pt, n values (Figure 3h) showed a positive correlation with the ORR activity (Figure 3g). For example, grain VII, which shows a high-index facet with [111] and [011] crystallographic characteristics, showed the highest ORR activity and n values. Meanwhile, grain VI and grain VIII, which showed the lowest ORR activity, had the lowest n values. Voltammetric movies showing the overall current and n value heatmap with continuous potential sweep are included as Movies S3 and S4. Grain VII shows both higher ORR activity and more H_2O_2 than grain VI, but the overall n value on grain VII (3.98) is higher than that on grain VI (3.96). The results suggest the importance of measuring both the activity and the product in determining selectivity. This small difference in n values also demonstrates that our probe can resolve as little as 0.5% difference in the mole fraction of H_2O_2.

The hybrid probe developed here has several advantages over SECM or SECCM alone. A confined electroactive substrate area is advantageous over pure SECM because the confinement of the droplet limits the lateral diffusion broadening and improves spatial resolution. In addition, the local substrate current is a direct measurement of electrochemical activity. Simultaneously quantifying the local activity and selectivity with no ambiguity of the local electrode area is an advancement to both techniques. This allows us to study the

dependence of electrocatalytic activity and selectivity on the crystal orientation, especially for facets that are not often accessible in single-crystal studies, like the one close to Au (411) that we have measured. Additionally, the sensitivity of the selectivity resulting from the proximity of the tip electrode to the substrate allows distinguishing <1% mole fraction differences in the products, as demonstrated in the ORR at different facets of Pt.

In summary, we developed a scanning electrochemical probe method that allows spatially resolved simultaneous mapping of both activity and selectivity for ORR via a hybrid SECCM–SECM probe. The probe shows high collection efficiency (>95%) as verified by voltammetric experiment and finite element simulation. Electrochemical mapping using this hybrid probe on polycrystalline Au and Pt samples and colocalized EBSD reveals a correlation between the ORR activity and selectivity and the crystallographic orientation. Less than 1% (mole fraction) difference in the ORR product is distinguished at different Pt facets, demonstrating the high sensitivity of product detection.

We expect that this method can be readily applied to other electrocatalysts to reveal the heterogeneity in the reactivity. In addition, the new method can be used to study the heterogeneity of selectivity and activity at the single-particle level by mapping the nanocatalysts sparsely dispersed on an inert substrate so that the droplet contact area only contains one particle at some locations.[8,13,21] Furthermore, the probe can be functionalized to extend the selectivity mapping to other reactions and products. The ability to unambiguously associate the activity and selectivity with well-defined electroactive areas (e.g., footprints observed in SEM) can facilitate the discovery of essential structural motifs that control the reactivity of electrocatalytic surfaces.

Supplementary Material

Refer to Web version on PubMed Central for supplementary material.

ACKNOWLEDGMENTS

We acknowledge the support from the National Institute of General Medical Sciences (1R35GM147172-01). Raluca Gearba and Andrei Dolocan at TMI and Xiaole Chen at CEC (supported by Welch Foundation H-F-0037) are acknowledged for aid with the facility and Deba Mandal for collecting the EBSD data. We are grateful for the opportunity to contribute to the field pioneered by Dr. Allen J. Bard. His legacy in electrochemistry inspires and guides our research.

REFERENCES

(1). Jin Z High-Spatiotemporal-Resolution Electrochemical Measurements of Electrocatalytic Reactivity. Anal. Chem. 2023, 95 (16), 6477–6489. [PubMed: 37023363]

(2). Polcari D; Dauphin-Ducharme P; Mauzeroll J Scanning Electrochemical Microscopy: A Comprehensive Review of Experimental Parameters from 1989 to 2015. Chem. Rev. 2016, 116 (22), 13234–13278. [PubMed: 27736057]

(3). Baker LA Perspective and Prospectus on Single-Entity Electrochemistry. J. Am. Chem. Soc. 2018, 140 (46), 15549–15559. [PubMed: 30388887]

(4). Ren H; Edwards MA Stochasticity in Single-Entity Electrochemistry. Curr. Opin. Electrochem. 2021, 25, 100632. [PubMed: 33102927]

(5). Ryu CH; Lee H; Lee H; Ren H Learning from the Heterogeneity at Electrochemical Interfaces. J. Phys. Chem. Lett. 2022, 13 (33), 7838–7846. [PubMed: 35976709]

(6). Bard AJ; Faulkner LR; White HS Scanning Electrochemical Microscopy. In Electrochemical Methods: Fundamentals and Applications, 3rd ed.; John Wiley & Sons, 2022; pp 819–850.

(7). Mariano RG; Kang M; Wahab OJ; McPherson IJ; Rabinowitz JA; Unwin PR; Kanan MW Microstructural Origin of Locally Enhanced CO2 Electroreduction Activity on Gold. Nat. Mater. 2021, 20 (7), 1000–1006. [PubMed: 33737727]

(8). Choi M; Siepser NP; Jeong S; Wang Y; Jagdale G; Ye X; Baker LA Probing Single-Particle Electrocatalytic Activity at Facet-Controlled Gold Nanocrystals. Nano Lett. 2020, 20 (2), 1233–1239. [PubMed: 31917592]

(9). Snowden ME; Güell AG; Lai SCS; McKelvey K; Ebejer N; O'Connell MA; Colburn AW; Unwin PR Scanning Electrochemical Cell Microscopy: Theory and Experiment for Quantitative High Resolution Spatially-Resolved Voltammetry and Simultaneous Ion-Conductance Measurements. Anal. Chem. 2012, 84 (5), 2483–2491. [PubMed: 22279955]

(10). Lu X; Li M; Peng Y; Xi X; Li M; Chen Q; Dong A Direct Probing of the Oxygen Evolution Reaction at Single $NiFe_2O_4$ Nanocrystal Superparticles with Tunable Structures. J. Am. Chem. Soc. 2021, 143 (41), 16925–16929. [PubMed: 34612638]

(11). Wahab OJ; Kang M; Unwin PR Scanning Electrochemical Cell Microscopy: A Natural Technique for Single Entity Electrochemistry. Curr. Opin. Electrochem. 2020, 22, 120–128.

(12). Hill JW; Hill CM Directly Mapping Photoelectrochemical Behavior within Individual Transition Metal Dichalcogenide Nanosheets. Nano Lett. 2019, 19 (8), 5710–5716. [PubMed: 31287956]

(13). Jeong S; Choi M-H; Jagdale GS; Zhong Y; Siepser NP; Wang Y; Zhan X; Baker LA; Ye X Unraveling the Structural Sensitivity of CO_2 Electroreduction at Facet-Defined Nanocrystals via Correlative Single-Entity and Macroelectrode Measurements. J. Am. Chem. Soc. 2022, 144 (28), 12673–12680. [PubMed: 35793438]

(14). Huang K; Shin K; Henkelman G; Crooks RM Correlating Surface Structures and Electrochemical Activity Using Shape-Controlled Single-Pt Nanoparticles. ACS Nano 2021, 15 (11), 17926–17937. [PubMed: 34730934]

(15). Li Y; Hu K; Yu Y; Rotenberg SA; Amatore C; Mirkin MV Direct Electrochemical Measurements of Reactive Oxygen and Nitrogen Species in Nontransformed and Metastatic Human Breast Cells. J. Am. Chem. Soc. 2017, 139 (37), 13055–13062. [PubMed: 28845981]

(16). Sánchez-Sánchez CM; Bard AJ Hydrogen Peroxide Production in the Oxygen Reduction Reaction at Different Electrocatalysts as Quantified by Scanning Electrochemical Microscopy. Anal. Chem. 2009, 81 (19), 8094–8100. [PubMed: 19725556]

(17). Zheng YL; Mei D; Chen Y-X; Ye S The Redox Reaction of Hydrogen Peroxide at an Au(100) Electrode: Implications for Oxygen Reduction Kinetics. Electrochem. Commun. 2014, 39, 19–21.

(18). Jirkovský JS.; Halasa M.; Schiffrin DJ. Kinetics of Electrocatalytic Reduction of Oxygen and Hydrogen Peroxide on Dispersed Gold Nanoparticles. Phys. Chem. Chem. Phys. 2010, 12 (28), 8042–8053. [PubMed: 20505889]

(19). Adžić RR; Strbac S; Anastasijević N Electrocatalysis of Oxygen on Single Crystal Gold Electrodes. Mater. Chem. Phys. 1989, 22 (3), 349–375.

(20). Aaronson BDB; Chen C-H; Li H; Koper MTM; Lai SCS; Unwin PR Pseudo-Single-Crystal Electrochemistry on Polycrystalline Electrodes: Visualizing Activity at Grains and Grain Boundaries on Platinum for the Fe^{2+}/Fe^{3+} Redox Reaction. J. Am. Chem. Soc. 2013, 135 (10), 3873–3880. [PubMed: 23405963]

(21). Li M; Ye K-H; Qiu W; Wang Y; Ren H Heterogeneity between and within Single Hematite Nanorods as Electrocatalysts for Oxygen Evolution Reaction. J. Am. Chem. Soc. 2022, 144 (12), 5247–5252. [PubMed: 35298886]

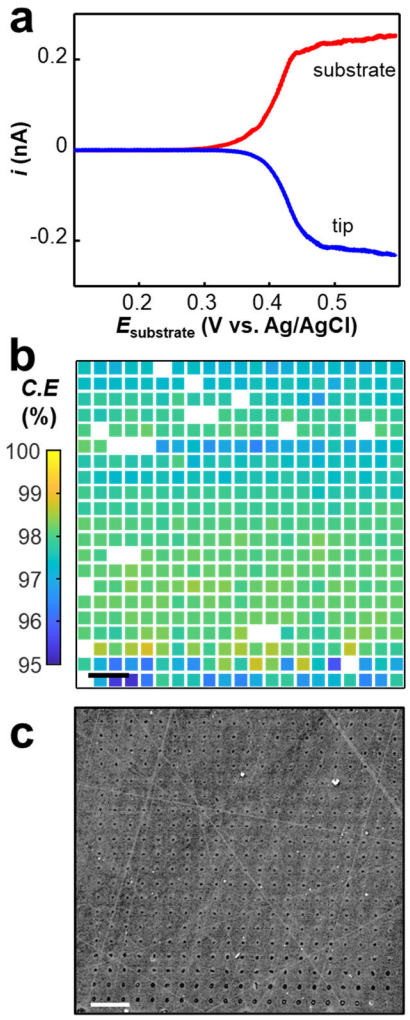

Figure 1.

(a) Linear sweep voltammogram for the $FcTMA^{+/2+}$ at one local point during mapping. Substrate potential ($E_{substrate}$) is swept positively while the tip is held at 0 V. (b) Collection efficiency (CE) heat map at 0.60 V vs Ag/AgCl. Collection efficiency is calculated by the ratio of substrate and probe current. (c) SEM image showing the footprints on the glassy carbon plate. The solution is 1 mM $FcTMA^{+}$ chloride and 10 mM phosphate buffer. The blank pixel in b indicates where the probe did not contact the substrate. Scale bars: 10 μm.

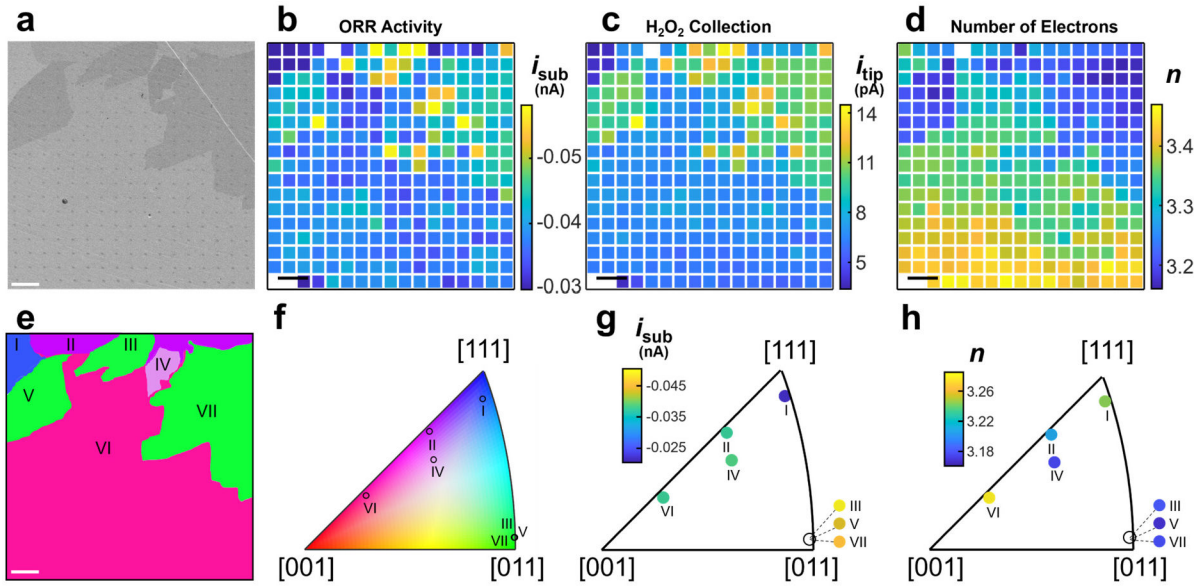

Figure 2.

(a) SEM image of polycrystalline Au with footprints after the electrochemical activity–selectivity mapping. Heat maps of (b) substrate current (i_{sub}) for ORR activity and (c) tip current (i_{tip}) for H_2O_2 collection. (d) ORR selectivity map measured by the average number of electrons (n) in ORR. (e) Colocalized EBSD crystal orientation map. (f) Inverse pole figure (IPF) showing the orientation of each grain. Stereographic triangles showing the grain-averaged (g) i_{sub} and (h) n at different crystal orientations. $E_{sub} = -0.42$ V, E_{tip}: 0.80 V (vs Ag/AgCl). Scale bars: 10 μm.

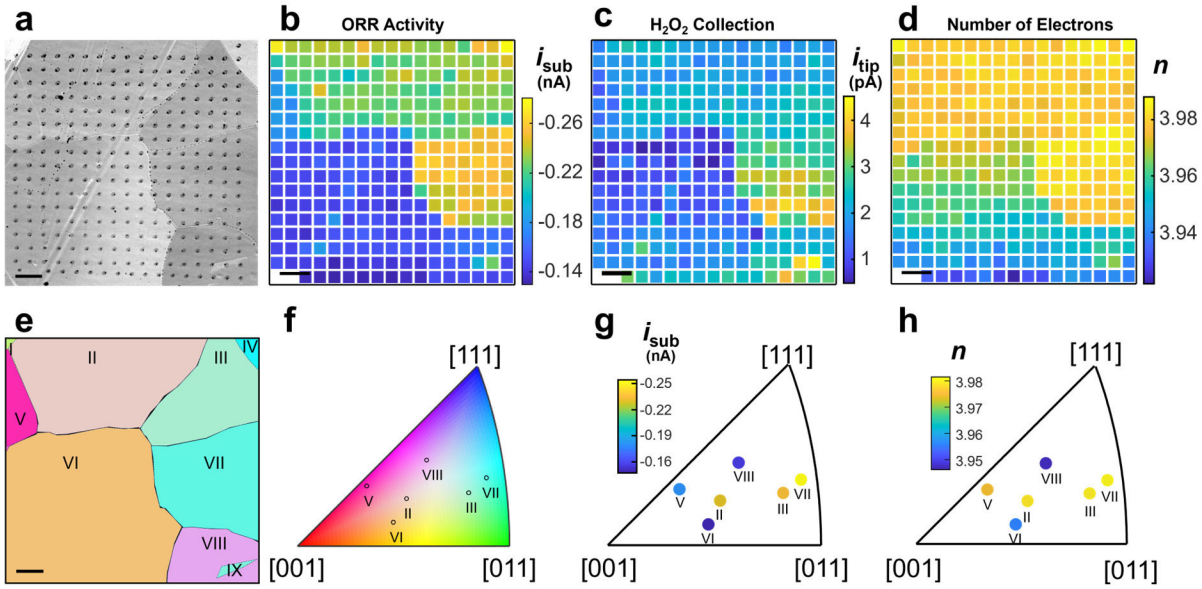

Figure 3.

(a) SEM image of polycrystalline Pt after the electrochemical activity–selectivity mapping. Heat maps of (b) substrate current (i_{sub}) for ORR activity and (c) tip current (i_{tip}) for H_2O_2 collection. (d) ORR selectivity map measured by the average number of electrons (n) in ORR. (e) Colocalized EBSD crystal orientation map. (f) IPF showing the orientation of each grain. Stereographic triangles showing the grain-averaged (g) i_{sub} and (h) n at different crystal orientations. i_{sub}: −0.50 V. E_{tip}: 0.80 V (vs Ag/AgCl). Scale bars: 10 μm. Grains containing <2 voltammetric measurements are excluded in the IPF.

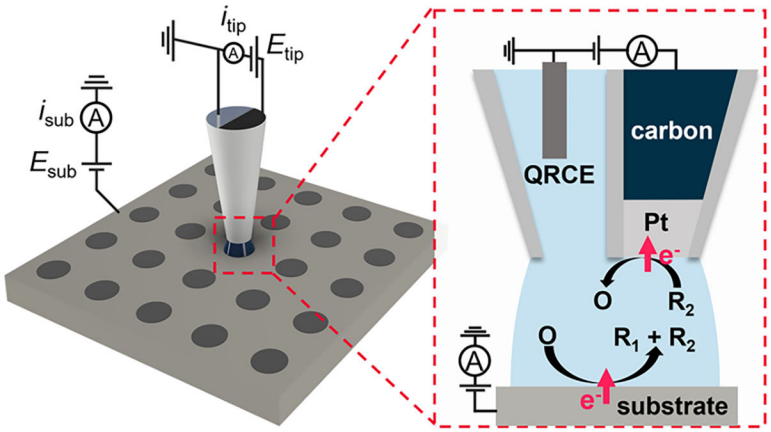

Scheme 1. Schematic Illustration of Hybrid SECCM-SECM Probe Used for Mapping the Local Electrocatalytic Activity and Selectivity